Generating False-Color Composites with a White-Light Optical Processor

F. T. S. Yu
Department of Electrical Engineering, The Pennsylvania State University, University Park, PA 16802
G. W. Petersen
Department of Agronomy and Office for Remote Sensing of Earth Resources, The Pennsylvania State University, University Park, PA 16802

ABSTRACT: A technique of false-color compositing by encoding multispectral remote sensing data with a low-cost white-light optical processor is described. Spatial encodings are made with various multispectral band image transparencies, and false-coloring is obtained by color filtering the smeared Fourier spectra. In contrast to the low-resolution digital image, the white-light method generates a high-quality color-coded product. This image is free from coherent artifact noise because coherent light sources are not used. This simple and versatile technique may offer a wide range of applications. Three bands of multispectral Landsat data were processed using 70-mm black-and-white film negatives. These false-color encoded images allowed for discrimination of various Earth surface features. Forests, agricultural lands, water, urban areas, and strip mines could be shown on the images as each of these thematic classes were displayed as a different color.

INTRODUCTION

MOST OPTICAL IMAGES used in scientific applications are gray-level density images, such as scanning electron microscopic images and x-ray transparencies. However, as has been shown for multispectral scanner images from satellites, color provides far greater visual discrimination.

In current practice, most false-color images are generated using digital computer techniques (Andrews *et al.*, 1972). Unfortunately, this method has three major drawbacks: (1) the equipment to generate these images is usually very expensive, (2) the technique is generally elaborate, and (3) image resolution is limited by the finite sample points of the system. A white-light false-color compositing technique that alleviates these three problems is described in this paper. The advantages of this new technique are (1) the cost of the equipment is substantially lower than for the digital process, (2) the encoder is relatively easy and economical to operate, and (3) the results of the optical technique can, in principle, match the resolution of the multispectral images.

In an earlier paper, the technique of false-color compositing with a white-light processing technique was described (Chao *et al.*, 1980). Although excellent results were reported using this method, false-color composites were obtained using only two primary colors. In this paper we shall extend the white-light false-color compositing technique to the multicolor case. For simplicity, we shall describe the case for three primary colors.

MATERIALS AND METHODS

Three bands of multispectral scanner Landsat data were processed for false-coloring using 70-mm black-and-white film negative transparencies. The bands were from the blue-green (Band 4: 0.5 to 0.6 μm), red (Band 5: 0.6 to 0.7 μm), and reflected infrared (Band 7: 0.8 to 1.1 μm) spectral regions. The scene is a 78 by 107 km subsample of Landsat scene 1440-15172 showing southeastern Pennsylvania (Figure 1). A multispectral-band image-encoding transparency was obtained by spatially sampling each of these three images onto black-and-white photographic film, with specific sampling grating frequencies oriented at specific azimuthal directions. To avoid the Moiré fringe pattern, these three images were sampled in orthogonal directions with different specific sampling frequencies, as shown in Figure 2. The intensity transmittance of the encoded film can be written as

$$\begin{aligned} T(x,y) = {} & K\{T_1(x,y)\,[1 + \operatorname{sgn}(\cos W_1 y)] \\ & + T_2(x,y)\,[1 + \operatorname{sgn}(\cos W_2 x)] \\ & + T_3(x,y)\,[1 + \operatorname{sgn}(\cos W_3 x)]\}^{\gamma} \end{aligned} \tag{1}$$

where K is an appropriate proportionality constant; T_1, T_2, and T_3 are the multispectral band transparencies, bands 4, 5, and 7, respectively; W_1, W_2, and W_3 are the respective carrier spatial frequencies; (x,y) is the spatial coordinate system of the encoded film; γ is the film gamma, and

$$\operatorname{sgn}(\cos x) \triangleq \begin{cases} 1, & \cos x \geq 0 \\ -1, & \cos x < 0 \end{cases} \tag{2}$$

PHOTOGRAMMETRIC ENGINEERING AND REMOTE SENSING, Vol. 52, No. 3, March 1986, pp. 367–371.

0099-1112/86/5203-367$02.25/0

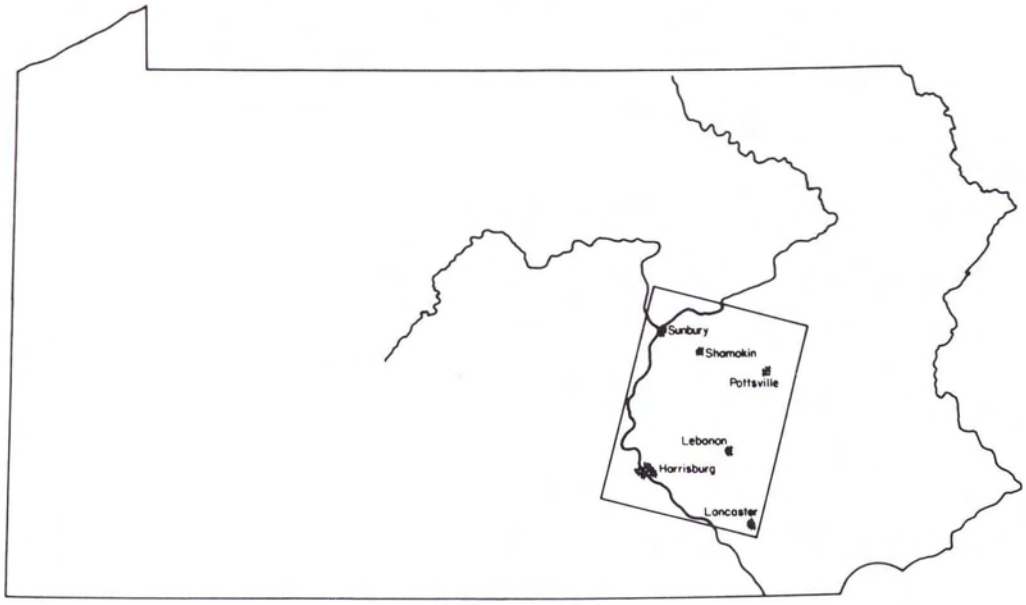

FIG. 1. Location map of the study site.

The encoded transparency was then bleached to obtain a surface relief phase object (Upatnicks and Leonard, 1969; Chang and Winick, 1980). We assume that the bleached transparency is encoded in the linear region of the diffraction efficiency versus the log exposure curve (Figure 3) (Chang and Winick, 1980). Thus, the amplitude transmittance of the bleached transparency can be written as

$$t(x,y) = \exp[i\phi(x,y)] \tag{3}$$

where $\phi(x,y)$ represents the phase delay distribution, which is proportional to the exposure of the encoded film (Smith, 1977), such that

$$\begin{aligned}\phi(x,y) = M\{&T_1(x,y)\,[1 + \operatorname{sgn}(\cos W_1 y)] \\ &+ T_2(x,y)\,[1 + \operatorname{sgn}(\cos W_2 x)] \\ &+ T_3(x,y)\,[1 + \operatorname{sgn}(\cos W_3 x)]\}\end{aligned} \tag{4}$$

where M is an appropriate proportionality constant. If we place this bleached encoded film at the input plane P_1 of a white-light optical processor (Yu, 1983), as illustrated in Figure 4, then the complex light distribution due to $t(x,y)$, for every λ, at the spatial frequency plane P_2, can be determined by the following Fourier transformation:

$$\begin{aligned}S(\alpha,\beta;\lambda) &= \iint t(x,y) \\ &\quad \exp\left[-i\frac{2\pi}{\lambda f}(\alpha x + \beta y)\right] dxdy \\ &= \iint \exp[i\phi(x,y)] \\ &\quad \exp\left[-i\frac{2\pi}{\lambda f}(\alpha x + \beta y)\right] dxdy\end{aligned} \tag{5}$$

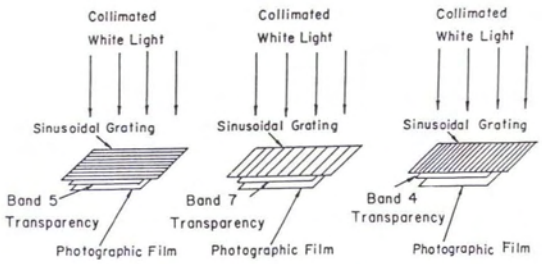

FIG. 2. Spatial encoding.

By expanding $t(x,y)$ into an exponential series, Equation 5 can be written as

$$\begin{aligned}S(\alpha,\beta;\lambda) = \iint\{&1 + i\phi(x,y) + \frac{1}{2}[i\phi(x,y)]^2 \\ &+ \ldots\} \exp\left[-i\frac{2\pi}{\lambda f}(\alpha x + \beta y)\right] dxdy\end{aligned} \tag{6}$$

By substituting Equation 4 into Equation 6 and retaining the first-order terms and the first-order convolution terms, we have

$$\begin{aligned}S'(\alpha,\beta,\lambda) &= \hat{T}_1\left(\alpha,\beta \pm \frac{\lambda f}{2\pi}W_1\right) \\ &+ \hat{T}_2\left(\alpha \pm \frac{\lambda f}{2\pi}W_2,\beta\right) + \hat{T}_3\left(\alpha \pm \frac{\lambda f}{2\pi}W_3,\beta\right) \\ &+ \hat{T}_1\left(\alpha,\beta \pm \frac{\lambda f}{2\pi}W_1\right) * \hat{T}_2\left(\alpha \pm \frac{\lambda f}{2\pi}W_2\beta\right)\end{aligned} \tag{7}$$

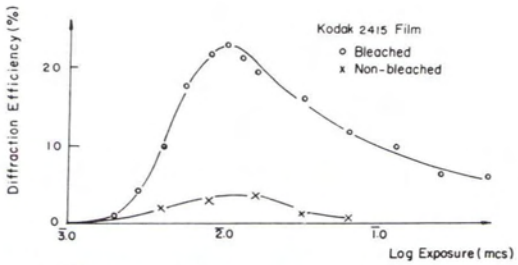

FIG. 3. Diffraction efficiency versus log exposure plot of a typical spatially-encoded film.

$$+ \hat{T}_1(\alpha,\beta \pm \frac{\lambda f}{2\pi} W_1) * \hat{T}_3(\alpha + \frac{\lambda f}{2\pi} W_3,\beta)$$
$$+ \hat{T}_2(\alpha \pm \frac{\lambda f}{2\pi} W_2,\beta) * \hat{T}_3(\alpha \pm \frac{\lambda f}{2\pi} W_3,\beta)$$

where $\hat{T}_1$, $\hat{T}_2$, and $\hat{T}_3$ are the Fourier transforms of T_1, T_2, and T_3 respectively; * denotes the convolution operation; and the proportional constants have been neglected for simplicity. We note that the last cross product term of Equation 7 would introduce a Moiré fringe pattern, which is in the same sampling direction of W_2 and W_3. Nevertheless, all of these cross product terms can be properly masked out at the Fourier plane. Thus, by proper color-filtering of the first-order smeared Fourier spectra, as shown in Figure 5, a Moiré-free false-color coded image can be obtained at the output plane P_3. The corresponding complex light field immediately behind the Fourier plane would be

$$S(\alpha,\beta) = \hat{T}_1(\alpha,\beta - \frac{\lambda_r f}{2\pi} W_1) + \hat{T}_2(\alpha - \frac{\lambda_b f}{2\pi} W_2,\beta) + \hat{T}_3(\alpha + \frac{\lambda_g f}{2\pi} W_3,\beta) \quad (8)$$

where λ_r, λ_b, and λ_g are the respective red, blue, and green color wavelengths. At the output image plane, the false-color coded image irradiance is, therefore,

$$I(x,y) = T_{1r}^2(x,y) + T_{2b}^2(x,y) + T_{3g}^2(x,y) \quad (9)$$

which is a superposition of three primary color encoded images, where T_{1r}, T_{2b}, and T_{3g} are the red, blue, and green amplitude distributions, respectively, of the three spatially encoded images. Thus, a Moiré-free color-coded image can be obtained at the output plane.

In our experiment, we used two sinusoidal sampling gratings for the spatial encodings, one with 26.7 lines/mm and the other with 40 lines/mm. The encoding transparency was made by Kodak Technical Pan Film 2415. The advantage of using this film is that it is a high resolution film and has a relatively flat spectral response. The plot of diffraction efficiency versus log exposure for Kodak 2415 film at 40 lines/mm sampling frequency is shown in Figure 3. From this figure, we see that bleached encoded films offer a higher diffraction efficiency — the optimum value occurs at exposures of 8.50×10^{-3} mcs. With this optimum exposure, it is possible to optimize the encoding process by first pre-ex-

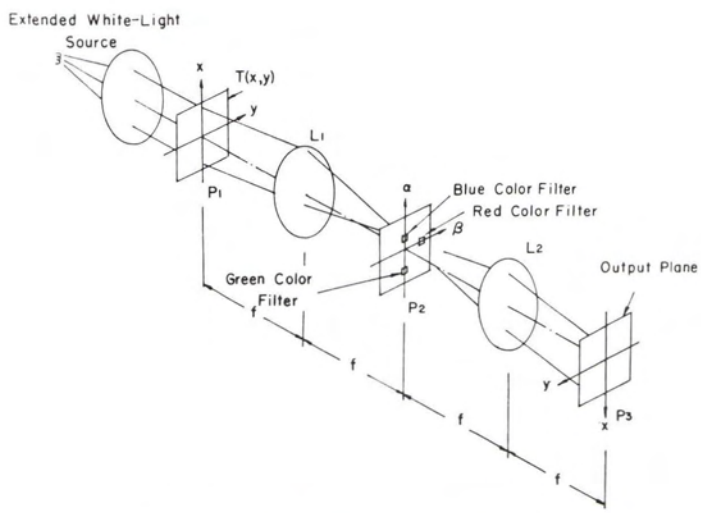

FIG. 4. A white-light false-color encoder.

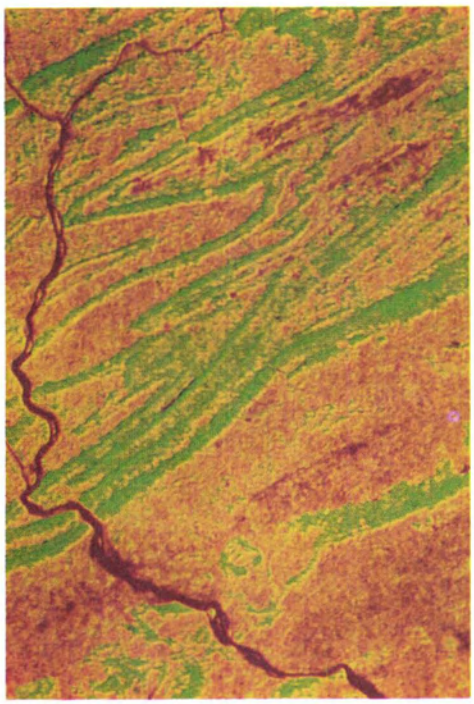

PLATE 1. Multispectral Landsat data with band 4 encoded green and band 5 encoded red.

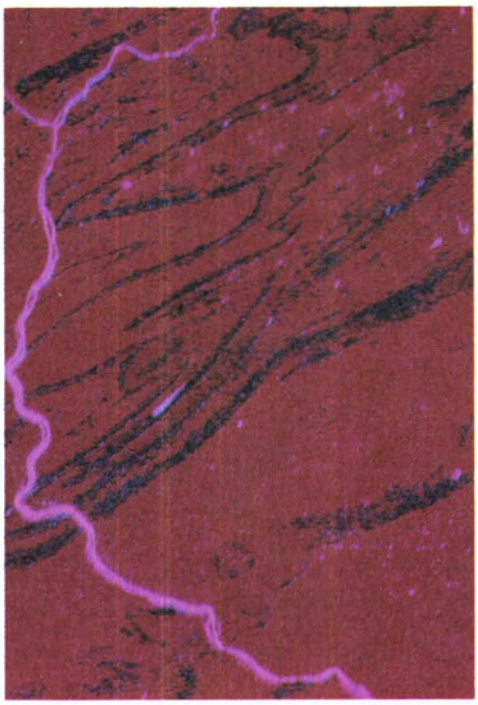

PLATE 2. Multispectral Landsat data with band 5 encoded red and band 7 encoded blue.

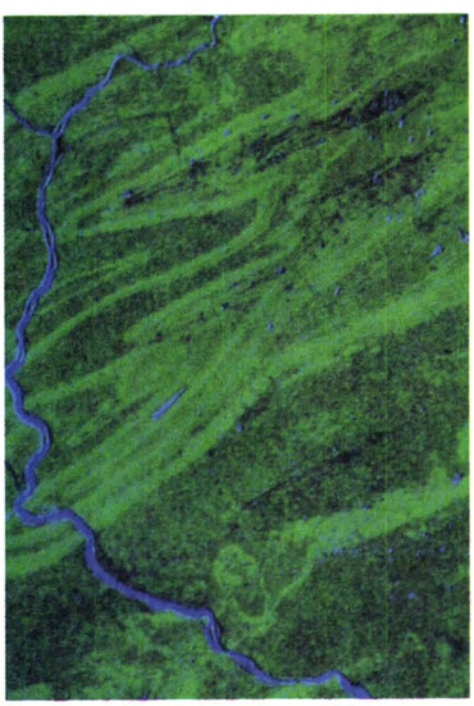

PLATE 3. Multispectral Landsat data with band 4 encoded green and band 7 encoded blue.

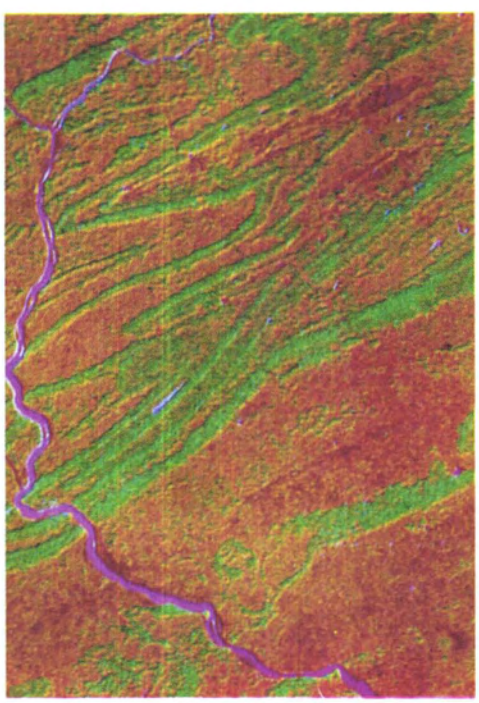

PLATE 4. Multispectral Landsat data with band 4 encoded green, band 5 encoded red, and band 7 encoded blue.

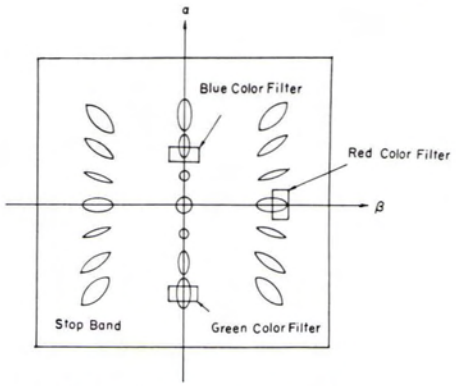

FIG. 5. Fourier plane color filtering.

posing the film beyond the toe region of the diffraction efficiency versus log exposure curve. Then the remaining exposure is subdivided into three regions, by taking into account the linear transmittant exposures of the three encoded images.

In false-color compositing, we use Kodak primary color filters 25, 47B, and 58 in the Fourier plane, as shown in Figure 5. A xenon-arc lamp is used as the extended white-light source for the false-color encoding technique shown in Figure 4.

RESULTS OF FALSE-COLOR ENCODING

The results of the false-color encoding of the Landsat multispectral scanner data are shown in Plates 1 through 4. In Plate 1, where band 4 is encoded green and band 5 is encoded red, the Susquehanna River and small bodies of water are delineated as deep red. The islands in the Susquehanna River are easily distinguished. Strip mines are dark red, urban areas (Harrisburg) are medium red, and agricultural lands are light red, orange, and yellow. Forested areas are green.

When red-encoded band 5 is combined with blue-encoded band 7 (Plate 2), the Susquehanna River is shown as a violet color. Small lakes and reservoirs appear as bluish hues. Some of the surface-mined areas appear as a light violet color, along with some of the bare fields in the agricultural valleys. The forested regions are dark blue and the agricultural areas are red. Urban areas are not delineated.

Water appears as several shades of blue when band 4 is encoded green, and band 7 is encoded blue (Plate 3). Northeast-southwest trending streams are also evident near the center of the image. Surface-mined areas are a much darker blue, and can be easily distinguished from water. Forested areas are most clearly distinguished on this image product as light green. The dark green areas are agricultural regions. Urban areas and strip development along major highways appear as dark blue to black in color.

When all three bands of the Landsat data are encoded (Plate 4), the Susquehanna River appears as violet, and the other bodies of water as shades of blue. The surface mines and urban areas are dark red. The agricultural valleys are orange and the forested regions are green.

The images presented in Plates 1 through 4 show the results of false-color encoding using a white-light optical processor. Six bands would be the practical limit for encoding. This approach for generating false-color composites has great potential. The white-light system is a high resolution color encoder. In principle, the resolution of the color encoded image can be as high as the original monochrome transparency. The white-light encoder is easy to construct and can be assembled for costs of less than $3,000. Once constructed, the system is also easy to operate. Therefore, this system offers a new and inexpensive approach to the development of false-color composites.

ACKNOWLEDGMENTS

Paper No. 6888 of the Journal Series of the Pennsylvania Agricultural Experiment Station. The authors would like to gratefully acknowledge the financial assistance of the Office of Scientific Research, U. S. Air Force, and the Office of Health and Environmental Research, U. S. Department of Energy.

REFERENCES

Andrews, H. C., A. B. Tescher, and R. P. Kruger, 1972. Image Processing by Digital Computer *IEEE Spectrum* 9:20–32.

Chang, B. J., and K. Winick, 1980. Silver-halide gelatin hologram *Society of Photo-optical Instrumentation Engineers* 215:172–177.

Chao, T. H., S. L. Zhuang, and F. T. S. Yu, 1980. White-light Pseudocolor Density Encoding Through Contrast Reversal. *Optical Letters* 5:230–232.

Smith, H. M., 1977. Basic Holographic Principles. Chapter 1 in *Holographic Recording Materials* (H. M. Smith, Ed.) Springer-Verlag, NY.

Upatnieks, J., and C. Leonard, 1969. Diffraction Efficiency of Bleached, Photographically Recorded Interference Patterns. *Applied Optics* 8:85–89.

Yu, F. T. S., 1983. *Optical Information Processing*. Wiley-Interscience Publishing Co., NY.

(Received 26 April, 1984; accepted 25 September 1985; revised 5 November 1985)